

HF-Diff: High-Frequency Perceptual Loss and Distribution Matching for One-Step Diffusion-Based Image Super-Resolution

Shoaib Meraj Sami^{1*}, Md Mahedi Hasan¹, Jeremy Dawson¹, Nasser Nasrabadi²,

¹West Virginia University, WV, USA ²Johns Hopkins University, MD, USA

Abstract

Although recent diffusion-based single-step super-resolution methods achieve better performance as compared to SinSR [57], they are computationally complex. To improve the performance of SinSR, we investigate preserving the high-frequency detail features during super-resolution (SR) because the downgraded images lack detailed information. For this purpose, we introduce a high-frequency perceptual loss by utilizing an invertible neural network (INN) pretrained on the ImageNet dataset. Different feature maps of pretrained INN produce different high-frequency aspects of an image. During the training phase, we impose to preserve the high-frequency features of super-resolved and ground truth (GT) images that improve the SR image quality during inference. Furthermore, we also utilize the Jensen-Shannon divergence between GT and SR images in the pretrained DINO-v2 embedding space to match their distribution. By introducing the high-frequency preserving loss and distribution matching constraint in the single-step diffusion-based SR (**HF-Diff**), we achieve a state-of-the-art CLIPQA score in the benchmark RealSR, RealSet65, DIV2K-Val, and ImageNet datasets. Furthermore, the experimental results in several datasets demonstrate that our high-frequency perceptual loss yields better SR image quality than LPIPS and VGG-based perceptual losses. Our code will be released in the repository at <https://github.com/shoaib-sami/HF-Diff>.

1. Introduction

Super-resolution (SR) is a well-known ill-posed problem in low-level computer vision. The primary goal of super-resolution is to improve the detailed information in degraded images. The degradation of the image can occur due to down-sampling, blurring, the effect of noise, and real-world degradation factors [59]. The degraded image contains structural information and lacks high-frequency detail information of an object [7, 70]. The main goal of SR is to recover the

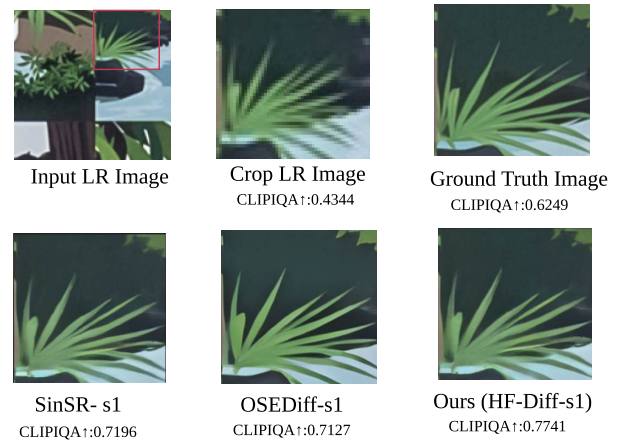


Figure 1. The visual and image quality comparison among the recent SOTA approaches (OSDiff [60] and SinSR [57]). We achieve the SOTA image perceptual quality (CLIPQA [51]) score.

missing information from the degraded image. Researchers use the generative adversarial network [21], normalizing flow [32], auto-regressive [15], transformer [31], and diffusion model-based algorithms [43] to solve the SR problem. However, diffusion-based SR outperforms the other techniques in several metrics [20, 51, 73]. Our paper aims to improve the single-step diffusion-based super-resolution algorithms for better performance than state-of-the-art (SOTA) SR methods [57, 60], which is crucial for different commercial [14, 77], academic [26, 34], medical science [38], and military [5, 27] applications.

Regarding model convergence, diffusion model-based SR algorithms [25, 56, 57, 60, 69] have advantages over the GAN-based SR [21]. The initial idea of diffusion-based super-resolution, SR3 [43], was proposed by employing low-resolution (LR) images inserted into the input of the denoiser in the diffusion model (DDPM [17]). However, SR3 performance drops if the degraded image comes from an unknown

*Corresponding author. Email: sms00052@mix.wvu.edu

distribution. To overcome this issue, SR3+ [42] was proposed using the self-supervised training strategy, a higher order degradation method, and noise conditioning augmentation. After that, the pretrained diffusion model and its modified reverse path were introduced using the transition distribution from the LR image to generate SR [68] image. These prior diffusion model-based SR algorithms require many computationally intensive sampling steps. ResShift [69] was proposed to overcome the computational complexity, which needs only 15 sampling steps and performs better than the earlier diffusion-based SR approaches. In that paper, the authors state that the reverse diffusion process starts from a bicubically interpolated LR image, and in each reverse step, the residual of the LR and HR image is dynamically integrated. To improve the SR inference process, the authors of SinSR [57] utilized deterministic sampling, similar to DDIM [46] in the teacher model. Then, they distill the teacher diffusion SR process to a student model in a single-step by maintaining better SR image quality than the teacher model. Our method also distills teacher information to the student model to accelerate the sampling procedure.

Recently, S3Diff [70] and OSEDiff [60], utilized the pretrained text-to-image (T2I) model’s information as a prior for the SR algorithm, and achieved better performance than SinSR [57]. Moreover, SinSR lags slightly in another widely used image quality metric (MUSIQ [20]) in several approaches [60, 71]. The CLIPQA [51] can capture semantic and abstract perception inside the image using the pretrained CLIP [40] model. However, MUSIQ can capture the perceptual quality of an image in multiple granularities. Our paper aims to improve the generated SR image’s semantic and abstract perception. To achieve this goal, we propose several novelties: i) we preserve the high-frequency features between super-resolution (SR) and ground-truth (GT) images, and ii) we match the distribution of GT and SR images during training.

Adversarial learning and classifier guidance are widely used in the diffusion model community for better image generation [11, 64]. One approach to stabilizing adversarial learning is to minimize the Jenson-Shannon divergence [33] between the distribution of perturbed original images and the diffusion model’s generated images [58]. Furthermore, in diffusion model literature, feature matching between real and generated image distributions has been extensively performed [7, 60, 66, 67]. The OSEDiff [60] employs KL divergence to regularize the latent space of GT and SR image distribution. The authors [7] introduced the nearest neighbor algorithm and a pretrained codebook to match the distorted low-resolution and SR image in embedding space. Inspired by these methods, we minimize the Jenson-Shannon (JS) divergence between the ground-truth HR image and the corresponding SR image, which yields better image quality. For this purpose, we use the SOTA self-supervised DINO-

v2 [35] pretrained encoder to extract embedding from GT and corresponding SR images and utilize JS divergence.

We propose a high-frequency perceptual loss to preserve the detail and fine-grained features in the student super-resolution model. There are different types of perceptual loss in the computer-vision literature [19, 39, 45]. We design an invertible neural network [4] (INN) and train it on the ImageNet-1K [10] dataset to calculate high-frequency perceptual loss. The INN-based high-frequency feature extractor is widely used in the visible-infrared image fusion literature [9, 62, 76]. However, to the best of our knowledge, we are pioneering the design of a high-frequency perceptual loss to preserve fine-grained and detailed features in image super-resolution. This pretrained high-frequency (HF) feature extractor calculates HF perceptual loss in the generated SR image and its corresponding GT image. By introducing high-frequency perceptual loss and distribution matching in the single-step super-resolution algorithm [57], we achieve a SOTA CLIPQA score by comparing recent SR algorithms [57, 60, 69] in four datasets.

The main contributions of our proposed super-resolution algorithm are:

- We propose a high-frequency preserving perceptual loss, which facilitates and enforces the network to maintain detail and fine-grained information.
- Our SR algorithm matches and aligns the GT and SR image distributions by minimizing the Jenson-Shannon divergence in the pretrained DINO-v2 embedding space.
- Our proposed method achieves state-of-the-art CLIPQA score in the RealSet65 [69], RealSR [6], ImageNet [10], DIV2K-Val [2], and DrealSR [37] datasets. In the DIV2K-Val and RealSR datasets, we achieve a better CLIPQA [51] score than the recent *OSEDiff* [60] algorithm. Furthermore, our method improves the qualitative visual representation compared to SOTA SR approaches.

2. Related Works

2.1. Image Super-Resolution

Super-resolution is a well-known low-level computer vision problem widely used in many applications [13, 59], such as surveillance [1], medical imaging [38], gaming [14], virtual reality [47], photography [36], face recognition [8], etc. After the evolution of AlexNet [23], researchers implemented deep learning-based super-resolution approaches [13, 19]. Following that, the generative adversarial network (GAN) evolved, and the GAN-based SR algorithms [24, 54, 71] were mainstream in the computer vision community [13]. The SR-GAN [24], ESRGAN [54], and RankSRGAN [74] are some well-known GAN-based super-resolution algorithms. The invertible neural network-based SRFlow [32] outperformed the GAN-based SR algorithms in 2020. Furthermore, the transformer [50] is the dominant network for

natural language processing, image classification, and detection, which facilitates the researchers to implement the transformer in super-resolution [31]. In addition, the denoising diffusion model beats the GAN in different perceptual metrics in the generative computer vision field [11]. The first denoising diffusion model-based SR algorithm was introduced in 2021 [43]. However, the diffusion-based SR algorithms initially faced slow sampling speeds and many inference steps [43, 69]. ResShift [69] was first algorithm able to sample high-quality super-resolution using a denoising diffusion model in only fifteen steps to overcome the slow sampling process. Recently, researchers [57, 60, 70] have successfully inferred the diffusion-based super-resolution in a single-step. Our paper improves the single-step diffusion-based SR algorithm that outperforms SOTA performance in some image quality metrics.

2.2. Analysis of Detailed Information in the Super-Resolution

In the super-resolution literature, pretrained VGG-16-based perceptual loss [19] is widely used to improve the SR image quality. In addition, Sims et al. [45] introduce frequency domain perceptual loss using discrete cosine transform [3] in the ground-truth and the SR image. Alongside perceptual loss, adversarial loss [13], neural texture transfer [63, 75], edge smoothness prior [49], gradient profile prior [48], edge and texture losses [39, 44] are used to achieve fine-grained information in the SR. For recovering texture information in the SR, the spatial feature transform and semantic segmentation are used in the CNN network [53].

In the subsequent section, we will discuss deterministic sampling [46] in the teacher model [57] and then delve into how our algorithm performs high-frequency perceptual loss and distribution matching. We also discuss other losses, e.g., distillation and inverse loss.

3. Methodology

In this section, we will first discuss deterministic sampling in the diffusion model. Then, we will elaborate on the proposed high-frequency perceptual loss and distribution alignment of the SR algorithm close to ground-truth image distribution.

3.1. Deterministic Sampling and Student Model

The earlier work for non-Markovian denoising deterministic sampling was introduced in the DDIM [46] paper. In the super-resolution literature, the SinSR [57] was pioneered in employing deterministic sampling. Inspired by SinSR, we employ deterministic sampling. The reverse deterministic sampling process $q(x_{t-1}|x_t, x_0, y)$ can be expressed by:

$$q(x_{t-1}|x_t, x_0, y) = \delta(g_\theta, x_t, y, t), \quad (1)$$

where δ represents the unit impulse function, y is the low-resolution image, x_0 is the ground-truth image and g_θ is

a pretrained ResShift [69] SR model. In the reverse process, the DDIM can calculate x_{t-1} from x_t using following equation:

$$x_{t-1} = a_t g_\theta(x_t, y, t) + b_t x_t + c_t y, \quad (2)$$

where a_t , b_t , and c_t are hyper-parameters. The detailed derivation of the hyper-parameters is described in the SinSR [57] paper.

The deterministic teacher model is illustrated in Figure 2. Where \mathcal{G}_θ is the T-step deterministic teacher network which predicts super-resolution output \hat{x}_0 from x_T state. We utilize the student model $\mathcal{G}_{\hat{\theta}}$ that learns the SR process from the teacher network (\mathcal{G}_θ) in a single-step. We utilized the vanilla distillation loss, consistency preserving, and inverse regularization losses from the SinSR [57].

The vanilla distillation loss can be described as:

$$\mathcal{L}_{distill} = \mathcal{L}_{MSE}(\mathcal{G}_{\hat{\theta}}(x_T, y, T), \mathcal{G}_\theta(x_T, y)), \quad (3)$$

vanilla distillation facilitates the student model learning of the T-step teacher SR model in a single-step. The student model ($\mathcal{G}_{\hat{\theta}}$) learns the deterministic teacher (\mathcal{G}_θ) mapping in a single step by employing vanilla distillation.

3.2. Matching the Super-Resolved and Ground-Truth Image Distribution

In the self-supervised learning benchmark, DINO-v2 [35] achieves promising performance, which interests us in extracting features of super-resolution (SR) and ground-truth (GT) images into the pretrained DINO-v2 space. We introduce aligning and matching the probability distribution of SR and GT images in DINO-v2 space. We align the probability distribution by using the Jenson-Shannon divergence [33]. Let P_{SR} and P_{GT} represent the probability distributions of the HR and SR images in the DINO-v2 embedding space. Then, the Jenson-Shannon divergence Loss ($\mathcal{L}_{JS-DINO}$) can be expressed as:

$$\begin{aligned} \mathcal{L}_{JS-DINO} &= \text{JSD}(P_{SR}||P_{GT}) \\ &= \frac{1}{2} [\text{KL}(P_{SR}||P_{Avg}) + \text{KL}(P_{GT}||P_{Avg})], \end{aligned} \quad (4)$$

where $P_{Avg}(x) = \frac{1}{2} [(P_{SR}(x) + P_{GT}(x))]$ and KL is Kullback-Leibler Divergence.

3.3. High-Frequency Perceptual Loss

The well-known implementation of perceptual loss is CNN-based [19, 73] framework; nevertheless, CNN does not provide lossless, invertible mapping between input and output. However, the invertible neural network (INN) [4] can maintain these properties and is widely used for high-frequency feature extraction [9, 62, 76]. In the image super-resolution

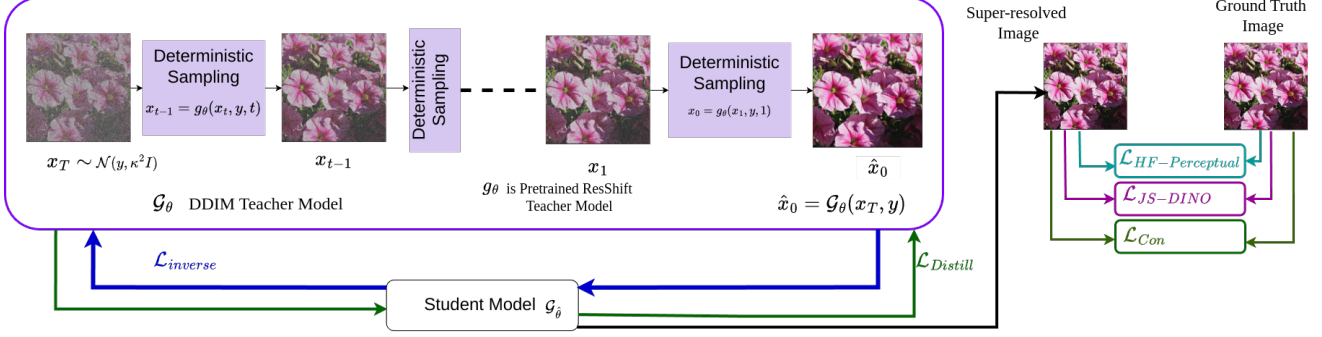


Figure 2. The training framework of HF-Diff. The low-resolution image is super-resolved by the multi-step deterministic teacher model (\mathcal{G}_θ). A student model (\mathcal{G}_δ) learns the deterministic teacher model by optimizing distill, high-frequency perceptual, distribution matching JS divergence, inverse, and consistency preserving losses.

domain, high-frequency image features are crucial because downgraded images lack detailed information. We introduce an invertible neural network-based high-frequency perceptual loss to compare and force the super-resolution algorithm to preserve the high-frequency (HF) feature [76]. For this purpose, we use an INN-based classifier (the details are shown in the Algorithm 2) pretrained on the ImageNet [10] dataset. For calculating HF perceptual loss, we preserve the spatial dimension of the feature map in the same way as the input. The different channels of INN can extract different perceptual detailed information about an image. We improve detailed information and perceptual image quality [51] by utilizing HF-perceptual loss. The invertible neural network consists of K numbers of invertible modules. The $(k+1)$ -th invertible module can be denoted as [76]:

$$\begin{aligned} \psi_{k+1}[n+1:N] &= \psi_k[n+1:N] + \mathcal{I}_1(\psi_k[1:n]), \\ \psi_{k+1}[1:n] &= \psi_k[1:n] \odot \exp(\mathcal{I}_2(\psi_{k+1}[n+1:N])) \\ &\quad + \mathcal{I}_3(\psi_{k+1}[n+1:N]), \\ \psi_{k+1} &= \mathcal{CAT}(\psi_{k+1}[1:n], \psi_{k+1}[n+1:N]), \end{aligned} \quad (5)$$

where \odot is the Hadamard product, $\psi_k[1:n] \in \mathbb{R}^{h \times w \times n}$ is the 1st to the n -th channels of the input feature for the k -th invertible layer ($k = 1, \dots, K$), the channel concatenation is denoted as $\mathcal{CAT}(\cdot)$ and \mathcal{I}_i ($i = 1, \dots, 3$) are three arbitrary mapping functions in each invertible layer. We utilize a two-layer CNN as an arbitrary mapping function in the invertible module. The invertible module is illustrated in Figure 3.

The ImageNet pretrained high-frequency feature extractor can be denoted as \mathcal{H} . The HF-perceptual loss can be expressed as follows:

$$\mathcal{L}_{HF-perceptual} = \mathcal{L}_{MSE}(\mathcal{H}(x_0), \mathcal{H}(\mathcal{G}_\delta(x_T))), \quad (6)$$

where GT and degraded LR image are x_0 and x_T , respectively. \mathcal{G}_δ is the one-step student model to generate SR. Figure 5 depicts different feature maps of the proposed INN-based feature extractor while calculating the perceptual loss.

The feature maps provide different aspects of the detailed features of a sample image.

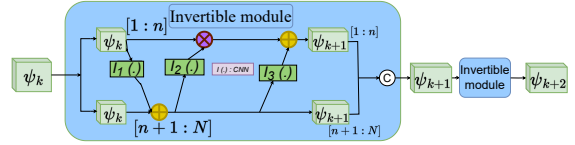


Figure 3. The illustration of an invertible module. The high-frequency feature extractor consists of K numbers of cascaded invertible modules [76]. The invertible module has an affine coupling layer [12] consisting of scaling and translation functions and a Hadamard product.

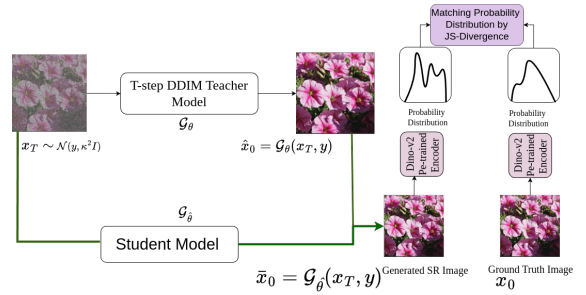


Figure 4. Depiction of distribution matching between ground-truth (GT) and super-resolved (SR) images. The distribution of GT and SR are matched by adopting Jensen-Shannon divergence into the pretrained DINO-v2 embedding space. The distribution matching constraint guides the student model in generating a more realistic SR image.

3.4. Regularization Loss

In the regularization loss [57], the student network (\mathcal{G}_δ) learns inverse mapping (\hat{x}_T) and generates synthetic ground-truth (\hat{x}_0) images. The inverse mapping loss can be denoted as:

$$\mathcal{L}_{inv} = \mathcal{L}_{MSE}(\mathcal{G}_\delta(\mathcal{G}_\theta(x_T, y), y), 0), x_T). \quad (7)$$

Algorithm 1 Training HF-Diff

Require: T step DDIM teacher model (\mathcal{G}_θ) and single-step student model ($\mathcal{G}_{\hat{\theta}}$).

Require: Paired training set (X, Y), where X and Y are the ground-truth and low-resolution image sets, respectively

- 1: $\mathcal{G}_{\hat{\theta}}$ is initialized by utilizing the pretrained model (\mathcal{G}_θ).
 - 2: **while** not converged **do**
 - 3: sample $x_0, y \sim (X, Y)$
 - 4: sample $\zeta \sim \mathcal{N}(\mathbf{0}, \kappa^2 \eta_T \mathbf{I})$
 - 5: $x_T = y + \zeta$
 - 6: $\hat{x}_0 = \mathcal{G}_\theta(x_T, y, T)$
 - 7: $\mathcal{L}_{distill} = L_{MSE}(\mathcal{G}_{\hat{\theta}}(x_T, y, T), \hat{x}_0)$
 - 8: $\mathcal{L}_{inv} = L_{MSE}(\mathcal{G}_{\hat{\theta}}(\hat{x}_0, y, 0), x_T)$
 - 9: $\hat{x}_T = \mathcal{G}_{\hat{\theta}}(x_0, y, 0)$,
 - 10: $\mathcal{L}_{Con} = L_{MSE}(\mathcal{G}_{\hat{\theta}}(\hat{x}_T, y, T), x_0)$
 - 11: $\mathcal{L}_{HF-Perceptual} = L_{MSE}(\mathcal{G}_{\hat{\theta}}(\hat{x}_T, y, T), x_0)$
 - 12: $\mathcal{L}_{JS-DINO} = L_{JS-Div.}(\mathcal{G}_{\hat{\theta}}(\hat{x}_T, y, T), x_0)$
 - 13: $\mathcal{L} = \mathcal{L}_{distill} + \mathcal{L}_{inv} + \mathcal{L}_{Con} + \mathcal{L}_{HF-Perceptual} + \mathcal{L}_{JS-DINO}$
 - 14: Perform a gradient descent step on $\nabla_{\hat{\theta}} \mathcal{L}$
 - 15: **end while**
 - 16: **return** The student model $\mathcal{G}_{\hat{\theta}}$.
-

The consistency preserving loss [57] (\mathcal{L}_{Con}) preserves the ground-truth information. First, the student model maps x_0 to \hat{x}_T and then again maps to $\hat{x}_0 = \mathcal{G}_{\hat{\theta}}(\mathcal{G}_{\hat{\theta}}(x_0, y, 0), y, T)$. The consistency preserving loss (\mathcal{L}_{Con}) minimizes the mean square error between \hat{x}_0 and x_0 .

$$\mathcal{L}_{Con} = \mathcal{L}_{MSE}(\mathcal{G}_{\hat{\theta}}(\mathcal{G}_{\hat{\theta}}(x_0, y, 0), y, T), x_0), \quad (8)$$

where, $\mathcal{G}_{\hat{\theta}}$ is the student model. The student model parameter $\hat{\theta}$ is initialized from the teacher parameter θ for faster convergence during training.

The comprehensive training objective. Our proposed framework optimizes the previously described five training objectives. The overall objective (\mathcal{L}_{Total}) can be denoted as:

$$\mathcal{L}_{Total} = \mathcal{L}_{distill} + \eta_1 \cdot \mathcal{L}_{HF-Perceptual} + \eta_2 \cdot \mathcal{L}_{JS-DINO} + \mathcal{L}_{inv} + \mathcal{L}_{Con}, \quad (9)$$

where η_1 , and η_2 are hyper-parameter. We set $\eta_1 = 0.2$, and $\eta_2 = 0.15$. The overall of the proposed HF-Diff is described in the Algorithm 1 and Figure 2.

4. Experiment

4.1. Experimental Setup

Training Details. We pursue the same model architecture and parameter setup as [57, 69]. We fine-tune the SinSR [57] model with two additional novel objectives. We train the HF-Diff model on ImageNet [10] dataset by following the

Algorithm 2 Pretraining of High-Frequency Feature Extractor

Require: Invertible module (ψ_k)-based feature extractor, CNN module (\mathcal{C}_l), fully connected layers (FC), shallow residual-block-encoder (\mathcal{RB}) for increasing feature maps from 3 to N.

Require: ImageNet training set (\bar{Z})

- 1: **while** not converged **do**
 - 2: sample $\bar{z} \sim (\bar{Z})$
 - 3: $z_1 = \mathcal{RB}(\bar{z})$
 - 4: **for** $k = 1, 2, \dots, K$ **do**
 - 5: $z_{k+1} = \psi_k(z_k)$
 - 6: **end for**
 - 7: $\hat{y}_1 = z_K$
 - 8: **for** $l = 1, 2, 3, \dots, L$ **do**
 - 9: $\hat{y}_{l+1} = \mathcal{C}_k(\hat{y}_l)$
 - 10: **end for**
 - 11: $y_{score} = \text{Soft-max}(\text{FC}(\hat{y}_L))$
 - 12: Perform a gradient descent step on $\nabla_{(\mathcal{RB}, \psi, \mathcal{C}, \text{FC})} \mathcal{L}$
 - 13: **end while**
 - 14: **return** The embedding of the K-th invertible module (z_K).
-

identical procedure same as ResShift [69] and SinSR [57]. Our paper pursues the real-world degradation pipeline from RealESRGAN [55].

Training High-Frequency Feature Extractor. We train a high-frequency feature extractor (based on an invertible neural network [76]) alongside convolutional and fully-connected layers to calculate HF-perceptual loss. Initially, we use a shallow residual block [16] to expand the image feature map from 3 to $N(= 128)$. The N channel of an image then passes through an invertible neural network. We take the output from the high-frequency feature extractor to calculate HF-perceptual loss. This network is trained on the ImageNet [10] dataset. We train this model for 20 epochs with a learning rate of $5e-4$ with a batch size of 32 and an exponential scheduler with a factor of 0.95 in every 5000 iterations. This model is optimized by Adam [22] optimizer.

Compared methods. We analyze the performance of our proposed method with several super-resolution algorithms, e.g., StableSR-s200 [52], RealSR-JPEG [18], DiffBIR-s50 [30], SeeSR-s50 [61], OSediff [60], PASD-s20 [65], ESRGAN [54], ResShift [69], SinSR [57], BSRGAN [71], SwinIR [28], RealESRGAN [55], DASR [29], and LDM [41]. We also evaluate and compare the inference time of ours with ResShift [69], SinSR [57], and OSediff [60].

Metrics. We employ PSNR, SSIM, and LPIPS [73] metrics for performance analysis in the testing dataset with reference images. Furthermore, we also utilize three widely used non-reference image quality metrics to evaluate SR images'

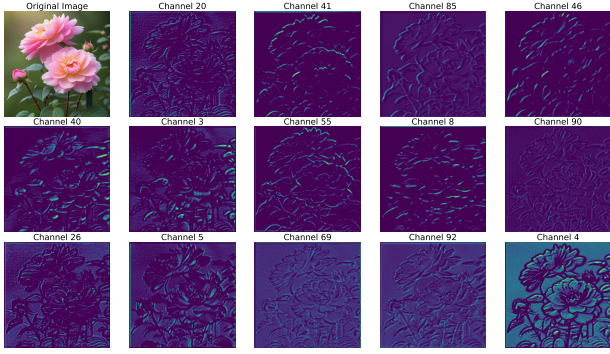


Figure 5. Visualization of detail feature maps of the pretrained INN extractor while calculating high-frequency perceptual loss. (Please zoom in on the figure for better perception.)

Methods	Datasets			
	<i>RealSR</i> [†]		<i>RealSet65</i>	
	CLIQQA [↑]	MUSIQ [↑]	CLIQQA [↑]	MUSIQ [↑]
ESRGAN [54]	0.2362	29.048	0.3739	42.369
RealSR-JPEG [18]	0.3615	36.076	0.5282	50.539
BSRGAN [71]	0.5439	63.586	0.6163	65.582
SwinIR [28]	0.4654	59.636	0.5782	63.822
RealESRGAN [6]	0.4898	59.678	0.5995	63.220
DASR [29]	0.3629	45.825	0.4965	55.708
LDM-15 [41]	0.3836	49.317	0.4274	47.488
ResShift-15 [69]	0.5958	59.873	0.6537	61.330
<i>SinSR-1</i> [57]	0.6887	61.582	0.7150	62.169
<i>HF-Diff-s1</i> (ours)	0.7240	61.897	0.7405	63.966

[†] RealSR is preprocess similar procedure as [57].

Table 1. Quantitative comparison among different super-resolution models on two real-world datasets. The best and the second best results among the SR methods are highlighted in **red** and **blue** colors, respectively.

realism and semantic coherence. These three image quality metrics are CLIPIQA [51], MUSIQ [20], and NIQE [72].

Training load. We train the HF-Diff network for 20K iterations with a batch size of 32. For this purpose, we initialized SinSR’s pretrained weight. The convergence of our algorithm (HF-Diff) is much faster; it takes about 20 hours.

4.2. Experimental Results and Comparison with State-of-the-Art

Quantitative comparisons on real-world datasets. We evaluate the performance of our proposed HF-Diff in the three real-world datasets RealSR [6], RealSet65 [69] and DrealSR [37]. The RealSet65 dataset contains 65 low-resolution images accumulated from different datasets and the Internet. The RealSR dataset has 100 real images captured by the ‘Nikon D810’ and the ‘Canon 5D3’ cameras. We investigate the image perceptual quality of HF-Diff

Methods	Metrics				
	PSNR [↑]	SSIM [↑]	LPIPS [↓]	CLIQQA [↑]	MUSIQ [↑]
ESRGAN [54]	20.67	0.448	0.485	0.451	43.615
RealSR-JPEG [18]	23.11	0.591	0.326	0.537	46.981
BSRGAN [71]	24.42	0.659	0.259	0.581	54.697
SwinIR [28]	23.99	0.667	0.238	0.564	53.790
RealESRGAN [55]	24.04	0.665	0.254	0.523	52.538
DASR [29]	24.75	0.675	0.250	0.536	48.337
LDM-30 [41]	24.49	0.651	0.248	0.572	50.895
LDM-15 [41]	24.89	0.670	0.269	0.512	46.419
ResShift-s15 [69]	24.90	0.673	0.228	0.603	53.897
SinSR-s1 [57]	24.56	0.657	0.221	0.611	53.357
<i>HF-Diff-s1</i> (ours)	24.31	0.645	0.225	0.660	55.323

Table 2. Quantitative comparison among widely used super-resolution models on *ImageNet-Test*. The best and second best results are highlighted in **red** and **blue**, respectively.

with other state-of-the-art super-resolution algorithms in Table 1 and 3. From Table 1, we achieve the best CLIPIQA [51] score among widely used GAN, Transformer, and diffusion model-based SR algorithms. Furthermore, HF-Diff achieves the second-best MUSIQ [20] score among different SR algorithms and better than the recent SinSR [57] methods. We also analyze the image quality metrics, e.g., NIQE, MUSIQ, and CLIPIQA, of the different diffusion model-based approaches with ours on DrealSR [37], and RealSR [60] datasets. In the RealSR dataset, HF-Diff achieves the best CLIPIQA score compared to others. However, in the DrealSR dataset, our approach gets slightly diminutive results. Furthermore, in the NIQE and MUSIQ metrics, SeeSR [61] and PASD [65] achieve better performance than ours because these are multi-step diffusion-based approaches that yield slightly better texture than a single-step inference [60].

Quantitative comparisons on synthetic datasets. We investigate the reference-based fidelity metrics (PSNR, SSIM) and non-reference-based image quality metrics (NIQE, MUSIQ, CLIPIQA) in the ImageNet-Test [10] and DIV2K-Val [2] datasets. From Table 2, our method achieves the best MUSIQ and CLIPIQA scores compared to the nine other SR approaches in the ImageNet-Test dataset. Our HF-Diff achieves the second-best LPIPS score. However, ours lags slightly in PSNR and SSIM metrics. We also find from Table 3 that ours achieves the second-best CLIPIQA score compared to the other seven diffusion-based SR approaches in the DIV2K-Val dataset. However, in NIQE and MUSIQ metrics, the SeeSR [61] and PASD [65] achieve better performance.

Qualitative comparisons. We visually compare our HF-Diff with recently introduced OSEDiff [60], SinSR [57], and other five super-resolution methods [28, 41, 55, 69, 71]. In three real-world samples, ours, OSEDiff, and RealESRGAN visually provide better depictions than others in Figure 6.

Computation and time complexity comparisons. We

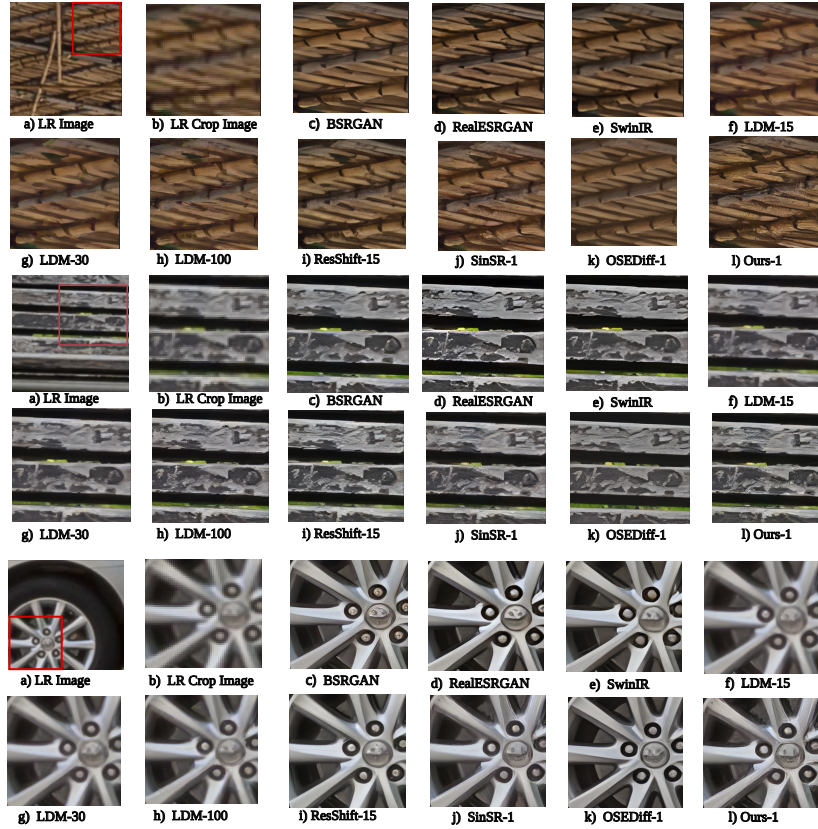


Figure 6. The visual comparison among different SOTA image super-resolution methods on some real-world samples.



Figure 7. The visual and perceptual quality improves by including high-frequency perceptual loss and distribution matching. We evaluate the perceptual quality by utilizing MUSIQ [20] and CLIP-IQA [51] metrics. Here, the ‘HF’ represents high-frequency perceptual loss, and ‘DM’ represents distribution matching.

investigate the inference time and parameters of recent diffusion-based super-resolution in our workstation with two NVIDIA-RTX ADA-6000 GPUs. For a fair comparison, we utilize the same image tensor ($128 \times 128 \times 3$). The model parameters and inference time of OSEDiff [60], SinSR [57], ResShift [69] and ours is reported in Table 5. HF-Diff can super-resolve images faster than OSEDiff [60] and ResShift [69].

4.3. Ablation Study

Effectiveness of high-frequency perceptual loss. The effectiveness of the proposed high-frequency perceptual loss can be deduced by both visual and quantitative comparison. From Figure 7, we can deduce that HF-perceptual loss improves the texture and fine-grained feature of the real-world sample images more than the SinSR [57]. Furthermore, this loss improves the MUSIQ and the CLIP-IQA scores between the two samples, as seen in Figure 7. From Table 4, we can infer that HF-perceptual loss significantly improves the NIQE, MUSIQ, and CLIP-IQA scores in the DIV2K-Val, RealSet65, and RealSR test sets.

Effectiveness of distribution matching. During training, we impose a constraint to match and align the ground truth and super-resolution image distribution in the DINO-v2 space. Figure 7 and Table 4 depict the importance of distribution matching in our HF-Diff method. From Figure 7, we can deduce that distribution matching improves the MUSIQ and the CLIP-IQA scores more than the vanilla SinSR. Also, this figure visually depicts that the distribution matching improves the image quality. From Table 4, we can deduce that the distribution matching constraint improves the NIQE, CLIP-IQA, and MUSIQ scores in all three datasets [2, 6, 69].

Table 3. Quantitative comparison among SOTA super-resolution methods on synthetic and real-world datasets. The best and the second best results of each metric are highlighted in **red** and **blue** colors, respectively. The number of reverse diffusion step is denoted as ‘s’.

Datasets	Methods	NIQE↓	MUSIQ↑	CLIQQA↑
DIV2K-Val	StableSR-s200 [52]	4.7581	65.92	0.6771
	DiffBIR-s50 [30]	4.7042	65.81	0.6704
	SeeSR-s50 [61]	4.8102	68.67	0.6936
	PASD-s20 [65]	4.3617	68.95	0.6788
	ResShift-s15 [69]	6.8212	61.09	0.6071
	SinSR-s1 [57]	6.0159	62.82	0.6471
	OSDiff-s1 [60]	4.7097	67.97	0.6683
	HF-Diff-s1 (ours)	5.9854	63.69	0.6822
DrealSR	StableSR-s200 [52]	6.5239	58.51	0.6356
	DiffBIR-s50 [30]	6.3124	61.07	0.6395
	SeeSR-s50 [61]	6.3967	64.93	0.6804
	PASD-s20 [65]	5.5474	64.87	0.6808
	ResShift-s15 [69]	8.1249	50.60	0.5342
	SinSR-s1 [57]	6.9907	55.33	0.6383
	OSDiff-s1 [60]	6.4902	64.65	0.6963
	HF-Diff-s1 (ours)	6.9863	58.66	0.6783
RealSR*	StableSR-s200 [52]	5.9122	65.78	0.6178
	DiffBIR-s50 [30]	5.5346	64.98	0.6463
	SeeSR-s50 [61]	5.4081	69.77	0.6612
	PASD-s20 [65]	5.4137	68.75	0.6620
	ResShift-s15 [69]	7.2635	58.43	0.5444
	SinSR-s1 [57]	6.2872	60.80	0.6122
	OSDiff-s1 [60]	5.6476	69.09	0.6693
	HF-Diff-s1 (ours)	6.3001	63.15	0.6840

* RealSR is preprocessed similar procedure as [60].

In summary, we can see that distribution matching is an important component in our HF-Diff super-resolution algorithm.

Effectiveness of utilizing the HF-perceptual loss and distribution matching simultaneously. We will visually and quantitatively investigate the importance of HF-perceptual loss and distribution matching simultaneously during training, as shown in Figure 7 and Table 4. From Figure 7, we can see that both objectives improve the texture and detailed information of the two sample images. Moreover, from Table 4, we can infer that both constraints improve the CLIP-IQA score significantly in two real-world [6, 69] and one synthetic [2] datasets.

Effectiveness of high-frequency perceptual loss compared to LPIPS and VGG-based perceptual loss. Table 4 shows that, in three datasets, our proposed HF-perceptual loss outperformed the three image quality metrics compared to LPIPS [73] and VGG-based perceptual loss [19]. For a fair comparison, we use the same settings and iteration number for all variations models in the ablation study.

5. Broader Impact and Limitation

By introducing our high-frequency perceptual loss and distribution alignment in the diffusion-based SR method, we

Table 4. Ablation study of proposed methods on synthetic and real-world three benchmark datasets. The best result is depicted in bold format. (‘HF’ represents the high-frequency perceptual loss, and ‘DM’ represents distribution matching during training.)

Datasets	Methods	NIQE↓	MUSIQ↑	CLIQQA↑
DIV2K-Val	SinSR-s1 [57]	6.02	62.82	0.6471
	HF-Diff(HF-only)	5.80	63.59	0.6724
	HF-Diff(DM-only)	5.83	63.16	0.6594
	HF-Diff(PL [†] -only)	5.97	61.94	0.6713
	HF-Diff(LPIPS ^{†‡} -only)	6.06	62.95	0.6638
	HF-Diff (HF+DM)	5.99	63.69	0.6822
RealSet65	SinSR-s1 [57]	5.98	62.17	0.7150
	HF-Diff(HF-only)	5.54	64.56	0.7315
	HF-Diff(DM-only)	5.66	64.19	0.7155
	HF-Diff(PL [†] -only)	5.63	62.64	0.7343
	HF-Diff(LPIPS ^{†‡} -only)	5.84	63.70	0.7295
	HF-Diff (HF+DM)	5.85	63.97	0.7405
RealSR*	SinSR-s1 [57]	6.29	60.80	0.6122
	HF-Diff(HF-only)	6.02	63.14	0.6684
	HF-Diff(DM-only)	6.18	62.42	0.6493
	HF-Diff(PL [†] -only)	6.15	62.43	0.6670
	HF-Diff(LPIPS ^{†‡} -only)	6.36	61.84	0.6580
	HF-Diff (HF+DM)	6.30	63.15	0.6840

* RealSR is preprocessed similar procedure as [60].

† VGG-based Perceptual Loss (PL) [19].

†† LPIPS loss [73].

Table 5. Time and parameter complexity comparison among some diffusion model-based SR algorithms. All the approaches are inferred in the same resource setting (NVIDIA-ADA-6000 GPU) and resolution of 128×128 .

	ResShift [69]	SinSR [57]	OSDiff [60]	Ours (HF-Diff)
Inference Step	15	1	1	1
Inference Time (s)	0.741	0.089	0.180	0.089
# Trainable Param (M)	118.6	118.6	8.5	118.6

achieve SOTA CLIP-IQA [51] scores in several datasets. We assume this novel perceptual loss can be employed in other super-resolution algorithms [24, 69] for better texture and detail feature generation.

The OSDiff [60] utilizes a large-scale pretrained text-to-image diffusion model as a prior that facilitates better MUSIQ [20] and NIQE [72] scores than ours but has a slower inference speed and lower CLIP-IQA score, as shown in Table 3 and 5.

6. Conclusion

We introduce novel perceptual loss to preserve high-frequency features during image super-resolution. For this purpose, we develop an invertible neural network-based high-frequency feature extractor. We also demonstrate that the high-frequency feature extractor captures different edges and detailed information. We also observe high-frequency perceptual loss attains better SR image quality than LPIPS and naive perceptual losses. Furthermore, we align and match the distribution of ground-truth and super-resolution images, which also improves the perceptual quality and visualization of super-resolution images. Introducing these novelties al-

lows the single-step diffusion-based super-resolution model to achieve the state-of-the-art performance on several image-quality metrics.

References

- [1] Andreas Aakerberg, Kamal Nasrollahi, and Thomas B Moeslund. Real-world super-resolution of face-images from surveillance cameras. *IET Image Processing*, 16(2):442–452, 2022.
- [2] Eirikur Agustsson and Radu Timofte. Ntire 2017 challenge on single image super-resolution: Dataset and study. In *The IEEE Conference on Computer Vision and Pattern Recognition (CVPR) Workshops*, 2017.
- [3] N. Ahmed, T. Natarajan, and K.R. Rao. Discrete cosine transform. *IEEE Transactions on Computers*, C-23(1):90–93, 1974.
- [4] Lynton Ardizzone, Jakob Kruse, Sebastian Wirkert, Daniel Rahner, Eric W Pellegrini, Ralf S Klessen, Lena Maier-Hein, Carsten Rother, and Ullrich Köthe. Analyzing inverse problems with invertible neural networks. *arXiv preprint arXiv:1808.04730*, 2018.
- [5] Harika Bandarupally, Harshitha Reddy Talusani, and T Sridevi. Detection of military targets from satellite images using deep convolutional neural networks. In *2020 IEEE 5th International Conference on Computing Communication and Automation (ICCCA)*, pages 531–535. IEEE, 2020.
- [6] Jianrui Cai, Hui Zeng, Hongwei Yong, Zisheng Cao, and Lei Zhang. Toward real-world single image super-resolution: A new benchmark and a new model. In *Proceedings of the IEEE/CVF International Conference on Computer Vision*, pages 3086–3095, 2019.
- [7] Chaofeng Chen, Xinyu Shi, Yipeng Qin, Xiaoming Li, Xiaoguang Han, Tao Yang, and Shihui Guo. Real-world blind super-resolution via feature matching with implicit high-resolution priors. In *Proceedings of the 30th ACM International Conference on Multimedia*, pages 1329–1338, 2022.
- [8] Jin Chen, Jun Chen, Zheng Wang, Chao Liang, and Chia-Wen Lin. Identity-aware face super-resolution for low-resolution face recognition. *IEEE Signal Processing Letters*, 27:645–649, 2020.
- [9] Jianjie Cui, Longfei Zhou, Fan Li, and Yufei Zha. Visible and infrared image fusion by invertible neural network. In *China Conference on Command and Control*, pages 133–145. Springer, 2022.
- [10] Jia Deng, Wei Dong, Richard Socher, Li-Jia Li, Kai Li, and Li Fei-Fei. ImageNet: A large-scale hierarchical image database. In *2009 IEEE conference on computer vision and pattern recognition*, pages 248–255. Ieee, 2009.
- [11] Prafulla Dhariwal and Alexander Nichol. Diffusion models beat GANs on image synthesis. *Advances in neural information processing systems*, 34:8780–8794, 2021.
- [12] Laurent Dinh, Jascha Sohl-Dickstein, and Samy Bengio. Density estimation using Real NVP. In *International Conference on Learning Representations*, 2022.
- [13] Chao Dong, Chen Change Loy, Kaiming He, and Xiaoou Tang. Image super-resolution using deep convolutional networks. *IEEE transactions on pattern analysis and machine intelligence*, 38(2):295–307, 2015.
- [14] Tingxing Tim Dong, Hao Yan, Mayank Parasar, and Raun Krusch. RenderSR: A lightweight super-resolution model for mobile gaming upscaling. In *Proceedings of the IEEE/CVF Conference on Computer Vision and Pattern Recognition*, pages 3087–3095, 2022.
- [15] Baisong Guo, Xiaoyun Zhang, Haoning Wu, Yu Wang, Ya Zhang, and Yan-Feng Wang. LAR-SR: A local autoregressive model for image super-resolution. In *Proceedings of the IEEE/CVF Conference on Computer Vision and Pattern Recognition*, pages 1909–1918, 2022.
- [16] Kaiming He, Xiangyu Zhang, Shaoqing Ren, and Jian Sun. Deep residual learning for image recognition. In *Proceedings of the IEEE conference on computer vision and pattern recognition*, pages 770–778, 2016.
- [17] Jonathan Ho, Ajay Jain, and Pieter Abbeel. Denoising diffusion probabilistic models. In *Advances in Neural Information Processing Systems*, pages 6840–6851. Curran Associates, Inc., 2020.
- [18] Xiaozhong Ji, Yun Cao, Ying Tai, Chengjie Wang, Jilin Li, and Feiyue Huang. Real-world super-resolution via kernel estimation and noise injection. In *proceedings of the IEEE/CVF conference on computer vision and pattern recognition workshops*, pages 466–467, 2020.
- [19] Justin Johnson, Alexandre Alahi, and Li Fei-Fei. Perceptual losses for real-time style transfer and super-resolution. In *Computer Vision—ECCV 2016: 14th European Conference, Amsterdam, The Netherlands, October 11–14, 2016, Proceedings, Part II 14*, pages 694–711. Springer, 2016.
- [20] Junjie Ke, Qifei Wang, Yilin Wang, Peyman Milanfar, and Feng Yang. MUSIQ: Multi-scale image quality transformer. In *Proceedings of the IEEE/CVF International Conference on Computer Vision*, pages 5148–5157, 2021.
- [21] Jiwon Kim, Jung Kwon Lee, and Kyoung Mu Lee. Accurate image super-resolution using very deep convolutional networks. In *2016 IEEE Conference on Computer Vision and Pattern Recognition (CVPR)*, 2016.
- [22] Diederik P Kingma. Adam: A method for stochastic optimization. *arXiv preprint arXiv:1412.6980*, 2014.
- [23] Alex Krizhevsky, Ilya Sutskever, and Geoffrey E Hinton. ImageNet classification with deep convolutional neural networks. *Advances in neural information processing systems*, 25, 2012.
- [24] Christian Ledig, Lucas Theis, Ferenc Huszár, Jose Caballero, Andrew Cunningham, Alejandro Acosta, Andrew Aitken, Alykhan Tejani, Johannes Totz, Zehan Wang, et al. Photo-realistic single image super-resolution using a generative adversarial network. In *Proceedings of the IEEE conference on computer vision and pattern recognition*, pages 4681–4690, 2017.
- [25] Haoying Li, Yifan Yang, Meng Chang, Shiqi Chen, Huajun Feng, Zhihai Xu, Qi Li, and Yueting Chen. SRDiff: Single image super-resolution with diffusion probabilistic models. *Neurocomputing*, 479:47–59, 2022.
- [26] Juncheng Li, Zehua Pei, Wenjie Li, Guangwei Gao, Longguang Wang, Yingqian Wang, and Tiejong Zeng. A systematic survey of deep learning-based single-image super-resolution. *ACM Computing Surveys*, 56(10):1–40, 2024.

- [27] Wenchao Li, Boyang Zhang, Kefeng Li, Jianyu Yang, Junjie Wu, Yin Zhang, and Yulin Huang. Lrsd-admm-net: Simultaneous super-resolution imaging and target detection for forward-looking scanning radar. *IEEE Journal of Selected Topics in Applied Earth Observations and Remote Sensing*, 17:4052–4061, 2024.
- [28] Jingyun Liang, Jie Zhang Cao, Guolei Sun, Kai Zhang, Luc Van Gool, and Radu Timofte. SwinIR: Image restoration using swin transformer. In *Proceedings of the IEEE/CVF international conference on computer vision*, pages 1833–1844, 2021.
- [29] Jie Liang, Hui Zeng, and Lei Zhang. Efficient and degradation-adaptive network for real-world image super-resolution. In *European Conference on Computer Vision*, pages 574–591. Springer, 2022.
- [30] Xinqi Lin, Jingwen He, Ziyang Chen, Zhaoyang Lyu, Bo Dai, Fanghua Yu, Wanli Ouyang, Yu Qiao, and Chao Dong. Diff-BIR: Towards blind image restoration with generative diffusion prior. *arXiv preprint arXiv:2308.15070*, 2023.
- [31] Zhisheng Lu, Juncheng Li, Hong Liu, Chaoyan Huang, Linlin Zhang, and Tiejiong Zeng. Transformer for single image super-resolution. In *Proceedings of the IEEE/CVF conference on computer vision and pattern recognition*, pages 457–466, 2022.
- [32] Andreas Lugmayr, Martin Danelljan, Luc Van Gool, and Radu Timofte. SRFlow: Learning the super-resolution space with normalizing flow. In *Computer Vision–ECCV 2020: 16th European Conference, Glasgow, UK, August 23–28, 2020, Proceedings, Part V 16*, pages 715–732. Springer, 2020.
- [33] María Luisa Menéndez, JA Pardo, L Pardo, and MC Pardo. The Jensen-Shannon divergence. *Journal of the Franklin Institute*, 334(2):307–318, 1997.
- [34] Brian B Moser, Arundhati S Shanbhag, Federico Raue, Stanislav Frolov, Sebastian Palacio, and Andreas Dengel. Diffusion models, image super-resolution, and everything: A survey. *IEEE Transactions on Neural Networks and Learning Systems*, 2024.
- [35] Maxime Oquab, Timothée Darcet, Théo Moutakanni, Huy V Vo, Marc Szafraniec, Vasil Khalidov, Pierre Fernandez, Daniel HAZIZA, Francisco Massa, Alaaeldin El-Nouby, et al. DINOv2: Learning robust visual features without supervision. *Transactions on Machine Learning Research*.
- [36] Joonkyu Park, Sanghyun Son, and Kyoung Mu Lee. Content-aware local gan for photo-realistic super-resolution. In *Proceedings of the IEEE/CVF International Conference on Computer Vision*, pages 10585–10594, 2023.
- [37] Hannan Lu ZongYuan Zhan Qixiang Ye Wangmeng Zuo Liang Lin Pengxu Wei, Ziwei Xie. Component divide-and-conquer for real-world image super-resolution. In *Proceedings of the European Conference on Computer Vision*, 2020.
- [38] Zhongxi Qiu, Yan Hu, Xiaoshan Chen, Dan Zeng, Qingyong Hu, and Jiang Liu. Rethinking dual-stream super-resolution semantic learning in medical image segmentation. *IEEE Transactions on Pattern Analysis and Machine Intelligence*, 46(1):451–464, 2024.
- [39] Mohammad Saeed Rad, Behzad Bozorgtabar, Urs-Viktor Marti, Max Basler, Hazim Kemal Ekenel, and Jean-Philippe Thiran. SROBB: Targeted perceptual loss for single image super-resolution. In *Proceedings of the IEEE/CVF international conference on computer vision*, pages 2710–2719, 2019.
- [40] Alec Radford, Jong Wook Kim, Chris Hallacy, Aditya Ramesh, Gabriel Goh, Sandhini Agarwal, Girish Sastry, Amanda Askell, Pamela Mishkin, Jack Clark, et al. Learning transferable visual models from natural language supervision. In *International conference on machine learning*, pages 8748–8763. PMLR, 2021.
- [41] Robin Rombach, Andreas Blattmann, Dominik Lorenz, Patrick Esser, and Björn Ommer. High-resolution image synthesis with latent diffusion models. In *Proceedings of the IEEE/CVF conference on computer vision and pattern recognition*, pages 10684–10695, 2022.
- [42] Hshmat Sahak, Daniel Watson, Chitwan Saharia, and David Fleet. Denoising diffusion probabilistic models for robust image super-resolution in the wild. *arXiv preprint arXiv:2302.07864*, 2023.
- [43] Chitwan Saharia, Jonathan Ho, William Chan, Tim Salimans, David J Fleet, and Mohammad Norouzi. Image super-resolution via iterative refinement. *IEEE transactions on pattern analysis and machine intelligence*, 45(4):4713–4726, 2022.
- [44] George Seif and Dimitrios Androutsos. Edge-based loss function for single image super-resolution. In *2018 IEEE International conference on acoustics, speech and signal processing (ICASSP)*, pages 1468–1472. IEEE, 2018.
- [45] Shane D Sims. Frequency domain-based perceptual loss for super resolution. In *2020 IEEE 30th International Workshop on Machine Learning for Signal Processing (MLSP)*, pages 1–6. IEEE, 2020.
- [46] Jiaming Song, Chenlin Meng, and Stefano Ermon. Denoising diffusion implicit models. In *International Conference on Learning Representations*, 2020.
- [47] Fanny Spagnolo, Pasquale Corsonello, Fabio Frustaci, and Stefania Perri. Design of a low-power super-resolution architecture for virtual reality wearable devices. *IEEE Sensors Journal*, 23(8):9009–9016, 2023.
- [48] Jian Sun, Zongben Xu, and Heung-Yeung Shum. Image super-resolution using gradient profile prior. In *2008 IEEE conference on computer vision and pattern recognition*, pages 1–8. IEEE, 2008.
- [49] Jian Sun, Jiejie Zhu, and Marshall F Tappen. Context-constrained hallucination for image super-resolution. In *2010 IEEE Computer Society Conference on Computer Vision and Pattern Recognition*, pages 231–238. IEEE, 2010.
- [50] Ashish Vaswani, Noam Shazeer, Niki Parmar, Jakob Uszkoreit, Llion Jones, Aidan N. Gomez, Łukasz Kaiser, and Illia Polosukhin. Attention is all you need. In *Advances in Neural Information Processing Systems*, 2017.
- [51] Jianyi Wang, Kelvin CK Chan, and Chen Change Loy. Exploring clip for assessing the look and feel of images. In *Proceedings of the AAAI Conference on Artificial Intelligence*, pages 2555–2563, 2023.
- [52] Jianyi Wang, Zongsheng Yue, Shangchen Zhou, Kelvin CK Chan, and Chen Change Loy. Exploiting diffusion prior for

- real-world image super-resolution. *International Journal of Computer Vision*, pages 1–21, 2024.
- [53] Xintao Wang, Ke Yu, Chao Dong, and Chen Change Loy. Recovering realistic texture in image super-resolution by deep spatial feature transform. In *Proceedings of the IEEE conference on computer vision and pattern recognition*, pages 606–615, 2018.
- [54] Xintao Wang, Ke Yu, Shixiang Wu, Jinjin Gu, Yihao Liu, Chao Dong, Yu Qiao, and Chen Change Loy. ESRGAN: enhanced super-resolution generative adversarial networks. In *Proceedings of the European conference on computer vision (ECCV) workshops*, pages 0–0, 2018.
- [55] Xintao Wang, Liangbin Xie, Chao Dong, and Ying Shan. Real-ESRGAN: training real-world blind super-resolution with pure synthetic data. In *Proceedings of the IEEE/CVF international conference on computer vision*, pages 1905–1914, 2021.
- [56] Yufei Wang, Yi Yu, Wenhan Yang, Lanqing Guo, Lap-Pui Chau, Alex C Kot, and Bihan Wen. ExposureDiffusion: Learning to expose for low-light image enhancement. In *Proceedings of the IEEE/CVF International Conference on Computer Vision*, pages 12438–12448, 2023.
- [57] Yufei Wang, Wenhan Yang, Xinyuan Chen, Yaohui Wang, Lanqing Guo, Lap-Pui Chau, Ziwei Liu, Yu Qiao, Alex C Kot, and Bihan Wen. SinSR: Diffusion-based image super-resolution in a single step. In *Proceedings of the IEEE/CVF Conference on Computer Vision and Pattern Recognition*, pages 25796–25805, 2024.
- [58] Zhendong Wang, Huangjie Zheng, Pengcheng He, Weizhu Chen, and Mingyuan Zhou. Diffusion-GAN: Training gans with diffusion. In *The Eleventh International Conference on Learning Representations*.
- [59] Zhihao Wang, Jian Chen, and Steven CH Hoi. Deep learning for image super-resolution: A survey. *IEEE transactions on pattern analysis and machine intelligence*, 43(10):3365–3387, 2020.
- [60] Rongyuan Wu, Lingchen Sun, Zhiyuan Ma, and Lei Zhang. One-step effective diffusion network for real-world image super-resolution. *arXiv preprint arXiv:2406.08177*, 2024.
- [61] Rongyuan Wu, Tao Yang, Lingchen Sun, Zhengqiang Zhang, Shuai Li, and Lei Zhang. SeeSR: Towards semantics-aware real-world image super-resolution. In *Proceedings of the IEEE/CVF conference on computer vision and pattern recognition*, pages 25456–25467, 2024.
- [62] Jian Xu and Xin He. DAF-Net: A dual-branch feature decomposition fusion network with domain adaptive for infrared and visible image fusion. *arXiv preprint arXiv:2409.11642*, 2024.
- [63] Fuzhi Yang, Huan Yang, Jianlong Fu, Hongtao Lu, and Baining Guo. Learning texture transformer network for image super-resolution. In *Proceedings of the IEEE/CVF conference on computer vision and pattern recognition*, pages 5791–5800, 2020.
- [64] Ling Yang, Haotian Qian, Zhilong Zhang, Jingwei Liu, and Bin Cui. Structure-guided adversarial training of diffusion models. In *Proceedings of the IEEE/CVF Conference on Computer Vision and Pattern Recognition*, pages 7256–7266, 2024.
- [65] Tao Yang, Rongyuan Wu, Peiran Ren, Xuansong Xie, and Lei Zhang. Pixel-aware stable diffusion for realistic image super-resolution and personalized stylization. *arXiv preprint arXiv:2308.14469*, 2023.
- [66] Tianwei Yin, Michaël Gharbi, Taesung Park, Richard Zhang, Eli Shechtman, Fredo Durand, and William T Freeman. Improved distribution matching distillation for fast image synthesis. *arXiv preprint arXiv:2405.14867*, 2024.
- [67] Tianwei Yin, Michaël Gharbi, Richard Zhang, Eli Shechtman, Fredo Durand, William T Freeman, and Taesung Park. One-step diffusion with distribution matching distillation. In *Proceedings of the IEEE/CVF Conference on Computer Vision and Pattern Recognition*, pages 6613–6623, 2024.
- [68] Zongsheng Yue and Chen Change Loy. DiffFace: Blind face restoration with diffused error contraction. *IEEE Transactions on Pattern Analysis and Machine Intelligence*, 2024.
- [69] Zongsheng Yue, Jianyi Wang, and Chen Change Loy. ResShift: Efficient diffusion model for image super-resolution by residual shifting. *Advances in Neural Information Processing Systems*, 2023.
- [70] Aiping Zhang, Zongsheng Yue, Renjing Pei, Wenqi Ren, and Xiaochun Cao. Degradation-guided one-step image super-resolution with diffusion priors. *arXiv preprint arXiv:2409.17058*, 2024.
- [71] Kai Zhang, Jingyun Liang, Luc Van Gool, and Radu Timofte. Designing a practical degradation model for deep blind image super-resolution. In *Proceedings of the IEEE/CVF International Conference on Computer Vision*, pages 4791–4800, 2021.
- [72] Lin Zhang, Lei Zhang, and Alan C Bovik. A feature-enriched completely blind image quality evaluator. *IEEE Transactions on Image Processing*, 24(8):2579–2591, 2015.
- [73] Richard Zhang, Phillip Isola, Alexei A Efros, Eli Shechtman, and Oliver Wang. The unreasonable effectiveness of deep features as a perceptual metric. In *Proceedings of the IEEE conference on computer vision and pattern recognition*, pages 586–595, 2018.
- [74] Wenlong Zhang, Yihao Liu, Chao Dong, and Yu Qiao. RankSRGAN: Generative adversarial networks with ranker for image super-resolution. In *Proceedings of the IEEE/CVF international conference on computer vision*, pages 3096–3105, 2019.
- [75] Zhifei Zhang, Zhaowen Wang, Zhe Lin, and Hairong Qi. Image super-resolution by neural texture transfer. In *Proceedings of the IEEE/CVF conference on computer vision and pattern recognition*, pages 7982–7991, 2019.
- [76] Zixiang Zhao, Haowen Bai, Jianshe Zhang, Yulun Zhang, Shuang Xu, Zudi Lin, Radu Timofte, and Luc Van Gool. CDDFuse: Correlation-driven dual-branch feature decomposition for multi-modality image fusion. In *Proceedings of the IEEE/CVF conference on computer vision and pattern recognition*, pages 5906–5916, 2023.
- [77] Xiang Zhu, Hossein Talebi, Xinwei Shi, Feng Yang, and Peyman Milanfar. Super-resolving commercial satellite imagery using realistic training data. In *2020 IEEE International Conference on Image Processing (ICIP)*, pages 498–502. IEEE, 2020.